Band gap of the Ge(111)$c(2\times8)$ surface by scanning tunneling spectroscopy

R. M. Feenstra*
Department of Physics, Carnegie Mellon University, Pittsburgh, Pennsylvania 15213, USA

J. Y. Lee and M. H. Kang
Department of Physics, Pohang University of Science and Technology, Pohang 790-784, Korea

G. Meyer†
Paul Drude Institut für Festkörperelektronik, Hausvogteiplatz 5-7, 10117 Berlin, Germany

K. H. Rieder
Institut für Experimentalphysik, Freie Universität Berlin, Arnimallee 14, 14195 Berlin, Germany
(Received 31 October 2005; published 11 January 2006)

The surface band gap of the Ge(111)$c(2\times8)$ surface at low temperature is determined on the basis of scanning tunneling spectroscopy. Electrostatic potential computations permit evaluation of tip-induced band bending, from which a correction to the energy scale of the observed spectra is made. Parameter values in the computations are constrained by comparison of the observed spectrum with known spectral features, including high-lying conduction band features derived from first-principles computations. The surface band gap, lying between the bulk valence band maximum and the minimum of an adatom-induced surface band, is found to have a width of 0.49 ± 0.03 eV.

DOI: 10.1103/PhysRevB.73.035310 PACS number(s): 73.20.At, 71.20.Mq, 68.37.Ef

I. INTRODUCTION

Although scanning tunneling spectroscopy (STS) has been used to study the electronic states of many semiconductor surfaces, quantitative determination of the surface band gap is rarely attempted. A significant limitation in this type of work is the occurrence of *tip-induced band bending*, in which part of the electric field in the vacuum extends into the semiconductor sample itself, leading to uncertainty in the precise energy scale of the observed spectra.[1] This band bending can be evaluated by electrostatic simulations based on models for the vacuum tunnel junction.[2] Such models involve a minimum of three parameters, describing the probe tip radius, sample-tip separation, and contact potential (work function difference) between sample and tip, and if extrinsic states (arising from defects and/or disorder) are present on the surface then typically two additional parameters are needed. In any quantitative evaluation of tunneling spectra it is desirable to constrain the parameter values as much as possible by matching to known quantities. Then, to evaluate some unknown quantity of interest from the data, it is necessary to vary the parameters over any remaining ranges of uncertainty in their values.

In this work we consider the quantitative determination of the band gap of the Ge(111)$c(2\times8)$ surface based on STS data.[3] This surface has been the subject of previous study by a wide range of surface science probes. Its structure is known to consist of an array of *adatoms* and *rest-atoms*.[4] Equal numbers of adatoms and rest-atoms occur on the surface, so that charge transfer from the former to the latter leads to a surface band gap, with empty surface states being localized on the adatoms and filled states on the rest-atoms. Despite this knowledge of the surface structure, however, the electronic properties of the surface are not so well understood. The band of rest-atom-derived states is known from photoemission experiment to lie resonant with the valence band (VB), with peak energy at about 0.7 eV below the VB maximum (VBM),[5] but the position of the adatom-derived band is less well known. One early work based on surface photovoltage revealed bands of empty states with threshold energies near 0.4 and 0.45 eV above the VBM.[6] A more recent work utilizing low energy electron scattering indicated a *maximum* in the empty-state density at 0.48 eV above the VBM,[7] although the identity of both this feature and various additional features within the gap cannot be clearly identified in those spectra. The empty states have also been observed by inverse photoemission[8] but the width of the surface band gap was not determined in that work. Considering the recent interest in the Ge(111)$c(2\times8)$ surface as a model system for studies of both atomic manipulation and carrier transport,[3,9,10] a quantitative determination of the width of the surface band gap is called for.

For clarity we point out that the term *surface band gap* can be defined in two different ways for situations such as the present one in which one band of surface states extends into the bulk band gap but the other is totally degenerate with bulk bands. The surface gap can be taken as either the difference between the extremal energy within the bulk gap of the surface band relative to the opposing bulk band edge, or between the energy extrema of the empty and filled surface bands. Of course, when significant mixing of the resonant surface band occurs with the bulk band (so that the bulk band edge acquires significant surface character) then only the former definition is tenable. In any case we are using the former definition in this paper although, e.g., the latter has been used in discussions of the Ge(111)2×1 surface.[11,12]

In addition to the determination of the Ge(111)$c(2\times8)$ surface band gap a major motivation for this work is the

 ©2006 The American Physical Society

development of a general theory for describing tunneling spectra of semiconductor surfaces. One component of such a theory, namely, the electrostatic simulations mentioned above, has already been fully developed.[2,3] Within those models we further consider in this work the computation of tunnel currents. Although many of the techniques for computing tunnel current have been previously described,[1,13,14] we bring those together in this work in a way that allows a somewhat more general treatment of the problem than previously accomplished.

We have acquired tunneling spectra of the Ge(111)$c(2\times8)$ surface over the temperature range 7–61 K. Adatom- and rest-atom-derived features are clearly observed in the data, with a surface band gap extending between the VBM and the minimum of the adatom-derived states. In our prior work we reported the observation of an apparent gap in the spectra of about 0.60 V, and based on rather general considerations we estimated a band bending correction in the range 0.0–0.2 eV yielding a surface gap value of 0.5 ± 0.1 eV.[3] That prior work was mainly concerned with investigating *high-current* behavior of the tunneling spectra that apparently involved nonequilibrium carrier occupation, whereas in the present work we focus on *low-current* measurements for which the band bending can be quantified using detailed electrostatic computations. To constrain the parameter values in the computation we compare the energy of several known spectral features between experiment and theory. One of these known quantities in particular is the location of an observed linear-onset in conduction band (CB) state-density, which on the basis of first-principles theory is found to be associated with high-lying CB features of the Ge. With this constrained set of band bending models we then determine a range of band bending corrections that can be applied to the observed surface band gap, yielding a final value for the surface gap of 0.49 ± 0.03 eV.

This paper is organized as follows: In Sec. II we summarize the experimental results of our prior work. Section III presents the first-principles theoretical work used to identifying CB-related features in the surface state-density. In Sec. IV we undertake an analysis of the data, comparing experimentally determined band bending values with those obtained from the electrostatic simulations. This analysis is performed in Secs. IV A and IV B within a semiclassical framework in which only values of the potential (not the current) are needed. Then, in Sec. IV C we include quantum effects, thereby requiring detailed computations of the tunnel current. It turns out that the quantum effects are not large for this system, typically about 10 meV, but nevertheless this value cannot be obtained without explicit computation. In Sec. IV D we determine our final value for the surface band gap, taking into account the various sources of error in both the experiment and the simulations. The paper is summarized in Sec. V, including comments on the overall methodology of the work.

II. EXPERIMENTAL RESULTS

The experimental work leading to the observed tunneling spectra has been described previously,[3] and will not be repeated in detail here. In brief, scanning tunneling spectroscopy (STS) measurements were performed at temperature in the range 7–61 K. A lock-in amplifier is used to measure the conductance, with modulation voltage of 10–20 mV. The Ge(111)$c(2\times8)$ surfaces were formed by cleaving a *p*-type Ge sample with 2×10^{16} cm^{-3} doping concentration on a (111) crystal face, and then annealing the sample at a temperature of about 500 °C for a few minutes. Well-ordered domains of $c(2\times8)$ structure were formed in this manner. A typical diameter of the domains is 50 nm, with the edges of the domains surrounded by disordered arrangements of adatoms and rest-atoms.[15] These domain boundaries are observed to introduce electronic states, which we refer to as *extrinsic* states, that lie within the surface band gap separating the bulk VB maximum and the minimum of the band of *intrinsic* adatom-derived states associated with the $c(2\times8)$ structure.

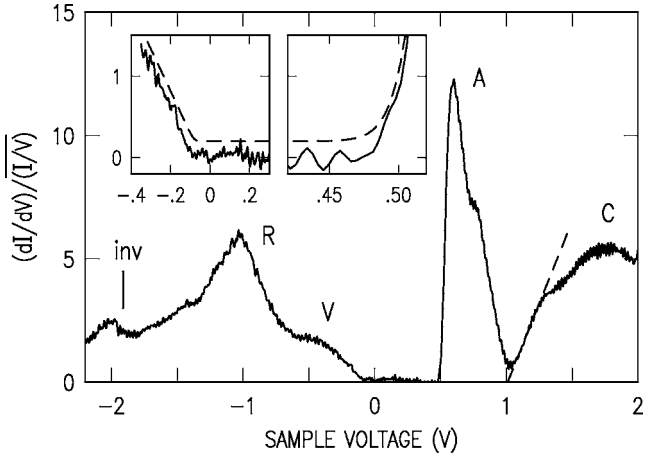

FIG. 1. Tunneling spectrum of the Ge(111)$c(2\times8)$ surface, acquired at 61 K. Insets show fitting of the onsets of the valence band and of the adatom surface band, to a function that assumes linear onset behavior modified by effects of temperature and modulation voltage.

A typical tunneling spectrum obtained from a well-ordered region of a $c(2\times8)$ domain is shown in Fig. 1, acquired at a temperature of 61 K. A number of features can be readily identified in the spectrum: A band gap is visible extending from about −0.1 to +0.5 V. The surface Fermi-level (0 V in the spectrum) is located near the bottom of the gap, as expected for *p*-type material. A large spectral peak is seen centered at about +0.7 V and it can be attributed to the empty states associated with the surface adatoms.[4,8,15] This spectral peak appears to have two components, consistent with the expectation of a splitting due to the two inequivalent types of adatoms in the $c(2\times8)$ structure.[16,17] In the filled states, at about −1.0 V, a spectral feature deriving from the surface rest-atoms is visible. This rest-atom band is resonant with VB states,[5] with the VBM seen in the spectrum at about −0.1 V. Finally, above the adatom band, at voltages above about +1.0 V, the current derives either from CB states or possibly from higher-lying surface bands. The observed surface gap is thus seen to be bounded by bulk VB states at its lower edge and surface adatom-derived states at its upper edge.

One additional feature occurs in the spectrum of Fig. 1, at about −1.9 V and labeled "inv." This feature arises from *inversion* of the carrier occupation at the surface, due to tip-induced band bending, with the bottom of the adatom band becoming occupied by electrons. Voltage-dependent imaging permits a definitive identification of this phenomenon,[3] and computations of inversion current in a spherical geometry provide a reasonable agreement with experiment in terms of the voltage at which the inversion occurs.

Curve fitting of the onsets of the VB and the adatom band have been carried out as described previously.[3] The functional form used assumes that the normalized conductance increases basically in a linear manner at the onsets, with some additional modification of the linear behavior due to the nonzero temperatures and the modulation voltage used in the experiment. The Appendix provides some justification of this functional form for the case of a bulk band (i.e., the VB in the present case), although for the adatom-derived surface band we use this form only because it provides a reasonably good fit to the data. The insets of Fig. 1 show the theoretical fits for the two onsets. Derived values for the onsets, based on the repeated measurements described in our prior work,[3] are -0.111 ± 0.011 V and 0.495 ± 0.003 V for the VB and adatom band, respectively, where the error values are the standard deviation of the mean.

III. FIRST-PRINCIPLES THEORETICAL RESULTS

For the purpose of evaluating the effects of tip-induced band bending on the observed spectra, it is necessary to have one or more features in the spectra that have *known* energies. With these, one can then use models of the band bending to interpolate or extrapolate between the known features in order to determine energies of other features (i.e., having unknown energies). In our observed spectrum of Fig. 1 there are two features in the filled states (negative sample voltages) that we can use for this purpose: the rest-atom peak and the location of the inversion voltage. However, there are no features on the empty states that can be immediately identified with electronic states of known energy. For the purpose of quantifying the surface band gap it is most useful to have a known energetic feature at positive sample voltage, since such a feature will aid in the interpolation procedure. For that reason we turn to a first-principles theoretical analysis of the spectrum of electronic surface states. Of course, it is well known that the computed energies of spectral features (particularly in the CB) can be substantially lower than the actual energies, and for this reason we do not rely on absolute energies from the computations. Rather, we seek some feature whose appearance can be matched between experiment and theory, and we then use the energy of this feature as expressed relative to *known* positions of high-lying conduction bands in the Ge.

Density-functional theory calculations were carried out using the generalized gradient approximation for the exchange-correlation potential[18] and norm-conserving pseudopotentials for the ionic potential.[19] We simulate the Ge(111)$c(2\times8)$ surface by a periodic slab geometry with a computationally feasible 2×2 surface unit cell: Each slab unit cell contains 18 layers of Ge atoms and a vacuum region of six empty layers. The bottom side of the slab is passivated by H atoms, and one Ge adatom is added on the top side, thus maintaining the same population ratio of adatoms and rest-atoms as the $c(2\times8)$ surface. The use of the reduced 2×2 surface representation is sufficient for the present surface electronic-structure analysis since we are interested not in absolute energy levels but only in the coupling of surface and bulk states, as will be discussed shortly. The electronic wave functions are expanded into plane waves with a cutoff energy of 15 Ry. The k-space integration is done using a 24×24 k-point mesh in the 2×2 surface Brillouin zone. Other computational details can be found elsewhere.[20]

Figure 2 shows the results of the bulk and surface electronic structure calculations. The calculated surface band structure shown in Fig. 2(b) represents well the projected bulk band structure and surface-derived electronic features: the rest-atom-derived band at around −0.5 eV, the adatom-derived band at around +0.5 eV, and high-lying resonance states produced by the coupling between the adatom band and the bulk conduction bands. These surface and resonance states give rise to noticeable features in the calculated surface density of states as shown in Fig. 2(c).

Let us now compare the theoretical results with the experimental spectrum. Referring again to Fig. 1, we observe above the adatom-derived surface band a linearly increasing density of states. This feature is marked by a dashed line in Fig. 1, with this line intersecting the horizontal axis at 1.01 ± 0.03 V. In the theoretical state-density of Fig. 2(c) we find a similar feature, also marked by a dashed line and with the intersection of that line on the vertical axis being 0.63 ± 0.04 eV. The origin of this linearly increasing feature can be ascertained by careful consideration of the conduction band structure of Ge. The CB minimum of bulk Ge occurs at the L-point of the Brillouin zone, with energy at low-temperatures of 0.744 eV relative to the VBM.[21] Higher-lying band extrema occur at the Γ-point and along the Δ direction (near the X-point) with nearly identical energies of 0.90 eV. In addition, a second band passes through the X-point with minimum (along the XK direction) very close to that of the X-point energy of 1.16 eV.[21]

From the theoretical results of Fig. 2, it is clear that the theoretical CB states associated with the Γ-valley minimum are strongly perturbed by the formation of the (111) reconstructed surface, i.e., those bulk states admix predominantly into the adatom band of the reconstructed surface. The linearly increasing portion of the theoretical state-density is seen to be composed primarily of states from the L-valley and the two X-valleys, with the observed onset of this feature in Fig. 2(c) lying midway between these bands. To determine a location of this onset relative to the *actual* band energies mentioned above, we note that the energies of the L-valley, the Δ direction, and the X-point given by the theory are 0.38, 0.73, and 0.91 eV, respectively, which are shifted relative to the above-mentioned actual values by 0.364, 0.17, and 0.25 eV, respectively. The average of these shifts is 0.261 eV, with a *maximum* spread of the shifts of about ±0.100 eV. We know from the theoretical results that all of the three bands make substantial contribution to the linearly increasing state density; assuming that their relative contri-

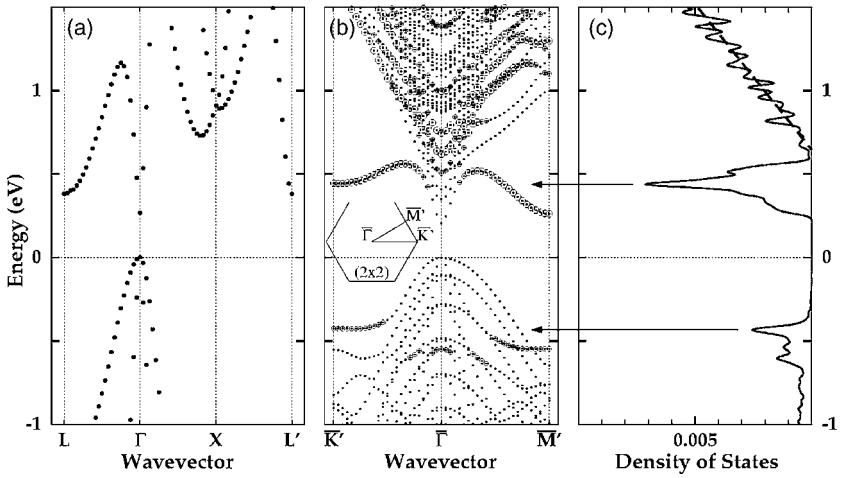

FIG. 2. (a) Bulk band structure of Ge along the symmetry lines connecting $L=2\pi/a(1/2,1/2,1/2)$, $X=2\pi/a(0,0,1)$, and $L'=2\pi/a(-1/2,-1/2,+1/2)$. The bulk lattice constant, a, was calculated as 0.578 nm. (b) Surface band structure of Ge(111)2×2: Large and medium open circles represent surface localized states containing more than 0.02% and 0.01%, respectively, of charge in the surface region of 0.45–0.55 nm away from the ideal first layer. (c) Surface density of states of Ge(111)2×2 obtained by integrating the local density of states over the surface region of 0.45–0.55 nm away from the ideal first layer. Arrows indicate the band-state origins of the state-density peaks. All energies are given relative to the VBM.

butions agree to within a factor of 2 we derive an error on the 0.261 eV shift of ±0.042 eV. We shift the theoretical value for the linearly increasing CB feature by the same amount, arriving at a corrected value of 0.891±0.058 eV (computing the error as the square root of the sum of the squares, as appropriate for uncorrelated errors).

IV. ANALYSIS

A. Tip-induced band bending

To relate the energies of spectral features to the sample-tip voltage at which they are observed, we must consider the effects of band bending within the semiconductor. We have previously presented a three-dimensional electrostatic simulation method whereby the potential distribution of the semiconductor-vacuum-metal system can be computed.[2] In particular, we obtain the electrostatic potential energy ϕ_0 at a point on the semiconductor surface directly opposite the tip apex. This *surface band bending* is measured relative to the potential energy at a point far inside the semiconductor. With $\phi_0\equiv0$ we would have the usual relationship between energy of a state E and the sample-tip voltage V, $E-E_F=eV$, where E_F is the Fermi level in the sample. With nonzero band bending this equation must be modified by shifting the energies by the surface band bending, as illustrated in Fig. 3(a), so that

$$E - E_F = eV - \phi_0. \tag{1}$$

In our simulations ϕ_0 is a function of the electrostatic potential energy of the probe-tip relative to a point far inside the semiconductor, ϕ_T, so that explicitly we have $\phi_0=\phi_0(\phi_T)$. The quantity ϕ_T equals $eV+\Delta\phi$, where $\Delta\phi$ is the *contact potential* defined as the work function of the tip minus that of the sample. Hence we have $\phi_0=\phi_0(eV+\Delta\phi)$.

Our electrostatic computations depend on a number of parameters, including sample-tip separation, tip radius-of-curvature, and contact potential. Additional parameters are needed to describe this Ge(111)$c(2\times8)$ surface since it is found that extrinsic states arising from disorder and/or defects on the surface play an important role in the electrostatics;[3] we adopt a model for these states in which the density per unit energy of such states is a *constant*. Above some energy known as the charge-neutrality level the states are assumed to be negative when filled and neutral when empty, and below this energy they are neutral when filled and positive when empty. In our prior work we cut off this extrinsic distribution of states at the VBM, with the rationale that below that energy the *resonant* states would be strongly mixed with bulk states and hence not sustain significant surface charge. In the present work however we allow the extrinsic states to maintain their charge character even at energies below the VBM. A correct description lies between

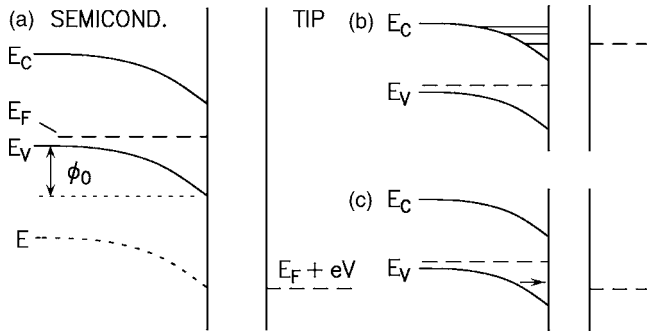

FIG. 3. (a) Sketch of energy bands used for computations of the electrostatic potential. The sample Fermi level is denoted by E_F with the tip Fermi level at E_F+eV where V is the sample-tip voltage. The band bending at the surface is denoted by ϕ_0, with V and ϕ_0 both being negative in this diagram. Quantum effects within the semiconductor can produce shifts in the observed band edges, as illustrated in (b) and (c) for localized state formation and for wave function tailing through a depletion region, respectively.

these two extremes, but the latter viewpoint is probably more appropriate in the present situation since the resonant states arise from dangling bonds which *do* maintain significant surface character, at least for energies not too far below the VBM.

Four quantities in the observed spectrum, Fig. 1, have known energies that we can use to constrain our parameters. First, the VB onset observed in the spectrum has, of course, a known energy; measuring all energies relative to the VBM this would be 0 eV. The band bending at this voltage of -0.111 ± 0.011 V would be thus be -0.101 ± 0.011 eV using a typical E_F value of 10 meV above the VBM.[22] The second known feature is the rest-atom spectral peak. This peak is observed to shift with tunnel current due to nonequilibrium effects in the occupation of extrinsic states,[3] but at low currents and relatively high temperatures these effects are small and the peak position is found to be -0.97 ± 0.05 V. In photoemission the energy of this state, at the Γ-point, was found to be about 0.85 eV below the VBM in some early work,[23] but at 0.66 ± 0.05 eV below the VBM in later work.[5] We consider the latter to be more reliable due to improved resolution and sample preparation and hence we use that value, yielding a band bending of -0.30 ± 0.07 eV (propagating the errors as the square root of the sum of the squares, as appropriate for these uncorrelated errors).

The third known spectral feature derives from the observed inversion voltage in Fig. 1 at -1.90 ± 0.03 V. In order for inversion of the Ge to occur the *minimum* magnitude band bending would be the E_F minus the surface gap, or -0.49 ± 0.11 eV using the estimated surface gap of 0.5 ± 0.1 eV from our previous work. However, our prior computations of inversion current indicate a delay in the onset of inversion since the inversion currents at this minimum band bending are negligible; for inversion currents near 1 pA and tip radii of about 30 nm this delay is 0.2 ± 0.1 V, thus yielding a band bending of -0.69 ± 0.15 eV. Finally, the theoretical results of Sec. III yield a band bending of 0.13 ± 0.11 eV at a voltage of 1.01 ± 0.03 V. All of these data points are pictured in the plot of Fig. 4.

We compute curves of the band bending vs. voltage, matching these to the data points of Fig. 4. We find that a best fit between the data and the simulations can be obtained with a single, unique set of parameters, namely, a tip radius of 30 nm, sample-tip separation of 0.9 nm (for relatively low current setpoints of about 10 pA), contact potential of -0.4 eV, extrinsic state density of 4×10^{12} cm^{-2} eV^{-1}, and charge neutrality level of -0.083 eV relative to the VBM. These values are listed in the first row of Table I. In the following section we justify this set of parameter values and we estimate error ranges for each of them. The solid line in Fig. 4, labeled *a*, shows the band bending vs. voltage for these best-fit parameter values. The band bending increases linearly up to about 0.3 V, at which point accumulation of holes in the Ge VB starts to occur and a corresponding decrease in slope of the curve is seen. Our goal is to determine the band bending that occurs at the observed onset of the adatom-band, at 0.495 ± 0.003 V. We denote this quantity $\phi_{0,A}$, as indicated by the horizontal dashed lines in Fig. 4.

The band bending analysis shown in Fig. 4 provides a very simple and direct illustration of the methodology of this paper. Essentially, we interpolate between several known band bending data points in order to determine the band bending $\phi_{0,A}$ at the onset of the adatom band. We follow this type of semiclassical analysis in the following section. However, we find that for a complete description of the problem

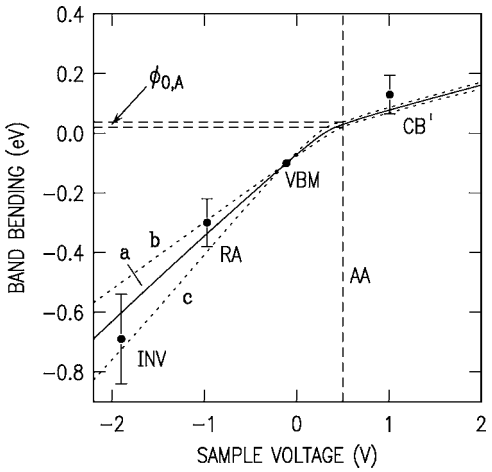

FIG. 4. Band bending in the semiconductor at a point opposite the probe tip apex, as a function of sample-tip voltage. Data points are shown for spectral features that have known energy such that the band bending can be absolutely determined (VBM, valence band maximum; RA, peak of rest-atom band; CB′, high lying conduction band feature; and INV, voltage at which inversion occurs). Theoretical curves interpolating between the data points are shown, with the solid line giving a typical result and the dotted lines giving maximal results consistent with the data. The vertical dashed line is located at the position of the observed onset of the adatom band (AA), with the horizontal dashed lines then giving the band bending at this voltage.

TABLE I. Various sets of values of the theoretical parameters, assuming a sample-tip separation of 0.9 nm, that produce a match between the simulations and the experimentally determined band bending values: tip radius R_T, density of extrinsic surface states σ, contact potential $\Delta\phi$, and charge neutrality level E_N relative to the VBM. Values of E_N are determined in the semiclassical analysis by matching to a band bending of -0.101 V at the VB onset voltage of -0.111 V, and in the quantum analysis values by matching to the VB onset voltage itself. The resulting band bending at a voltage of +0.495 V, corresponding to the onset of the adatom band, is listed as $\phi_{0,A}$.

			Semiclassical		Quantum	
R_T (nm)	σ (cm^{-2} eV^{-1})	$\Delta\phi$ (eV)	E_N (eV)	$\phi_{0,A}$ (meV)	E_N (eV)	$\phi_{0,A}$ (meV)
30	4×10^{12}	−0.4	−0.083	28	−0.004	21
10	4×10^{12}	−0.4	−0.008	20	0.050	4
100	4×10^{12}	−0.4	−0.186	38	−0.098	30
30	2×10^{12}	−0.4	−0.233	32	−0.072	25
30	7×10^{12}	−0.4	−0.018	23	0.029	11
30	4×10^{12}	−0.2	0.028	43	0.082	35
30	4×10^{12}	−0.6	−0.255	21	−0.111	5

we must take into account quantum effects that occur in the spectra, and those are discussed in Secs. IV C and IV D.

B. Variation of parameters

As described above, we have five parameters in our simulation theory. By matching our simulation results to the band bending at the VBM (which is quite accurately known) we can eliminate one parameter from our theory; we choose this to be the charge neutrality level. This parameter is highly correlated with the contact potential; varying either of these parameters produces primarily an upwards or downwards shift of the band bending curves in Fig. 4 (i.e., affecting the y intercept). Alternatively varying the extrinsic charge density causes the slope of the band bending curves to change, and varying the tip radius has a similar, though weaker, effect. The sample-tip separation affects both the slope and the y intercept, and we find it convenient to discuss this parameter in relation to the contact potential. In the discussion below we first focus on the values of tip radius and extrinsic charge density, and we then turn to the contact potential and sample-tip separation.

The values of tip radii consistent with experiment were estimated in our prior work on the basis of the observed inversion currents to be 10–100 nm,[3] and we continue to use this range for the present analysis. Using our best-fit values of contact potential and extrinsic state density, we compute the band bending that occurs for these extremal values of tip radii. These curve are shown as b and c in Fig. 4, and the parameter sets are listed in the second and third rows of Table I with the fifth column giving the respective $\phi_{0,A}$ values. Considering the extrinsic state density, we use our best-fit value for the tip radius of 30 nm and we evaluate the maximal values of band bending that are consistent with the data points of Fig. 4. The resulting band bending curves (not shown) fall quite close to b and c in Fig. 4, and the respective parameters are listed in the fourth and fifth rows of Table I.

With the ranges of tip radii and extrinsic state density determined as above, and considering for the moment a fixed sample-tip separation of 0.9 nm, the remaining parameter in the theory is the contact potential. As mentioned above the primary effect of the contact potential is to shift the band bending curves of Fig. 4 up or down, but since we are matching all of these to the observed VBM (i.e., by adjusting the charge neutrality level) then this effect is cancelled. A secondary influence of the contact potential is to affect the turnover of the band bending curves into the accumulation regime, and the resulting values of $\phi_{0,A}$ are thus affected. This effect is not large, but nevertheless we must somehow establish a range of contact potentials that are consistent with the experiment.

One means of constraining the values of contact potential is to examine the dependence of the band bending on separation, as determined in our prior work[3] and shown in Fig. 5. Some uncertainty in the zero of separation occurs for this data; in our prior work we estimated that zero such that the separation values were *lower* bounds on the actual values, but in the present work it is more relevant to give *upper* bounds on the separations. We thus shift our zero by 0.3 nm compared to that shown in our prior work; it is possible that the *actual* separations for the data shown in Fig. 5 are 0.1–0.2 nm *less* than that shown there but it is unlikely that they are greater than those shown.

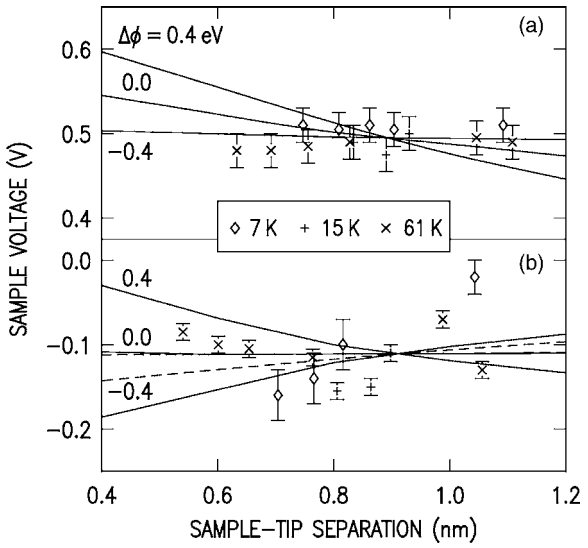

FIG. 5. Dependence of the onsets of (a) the adatom band and (b) the VB, as a function of the sample-tip separation. Data points show experimental results with the error bars representing the precision of curve fitting. Lines show simulated results for the contact potential values indicated, with solid lines showing semiclassical results and dashed lines quantum results.

Figure 5 compares the experimental results with the simulations for the separation dependence, using various contact potential values and with our best-fit values for the tip radius and extrinsic state density. The predicted onset voltages are obtained by solving Eq. (1) for the appropriate sample voltage corresponding to a given energy of the band minimum (0 eV for the VB, and for the adatom band the energies that, using Table I, yield an onset of 0.495 V). The solid lines in Fig. 5 show the results for this semiclassical analysis. In Fig. 5(a) we see that, not surprisingly, positive contact potentials produce a rather large dependence of the adatom band edge on separation whereas values near −0.4eV yield little dependence on separation, the latter case corresponding to nearly flat band conditions at the voltage corresponding to the adatom band edge. Comparing the simulation results with the experiment we thus estimate a range of possible contact potentials of about -0.4 ± 0.2eV. For the VBM, Fig. 5(b), there is more scatter in the data due most likely to variations in the density of extrinsic states across the surface. Also, for the VBM onsets, quantum effects turn out to be quite significant so we defer further analysis of Fig. 5(b) until after discussion of those effects.

C. Tunneling current-voltage characteristics

Equation (1) of the preceding section is based on the semiclassical notion of band bending. This type of analysis should work well for *surface* states since they are localized near the surface, but for *bulk* bands some additional quantum

effects must be considered. For tunneling into a bulk VB or CB two types of quantum effects can shift a band onset away from the position given by Eq. (1). First, as shown in Fig. 3(b), states that are localized in the direction perpendicular to the surface can form, i.e., for band bending that is downwards for a CB or upwards for a VB. Such localized states can potentially shift the observed onset of a band, e.g., by the energy of the lowest localized state relative to the band minimum at the surface. However, in the present system of interest we need not be concerned with such effects since it is the adatom-derived *surface* states that contribute to the onset of the empty-state band in our observed spectra. We therefore do not further consider this particular effect here.

The second type of quantum effect that can be important in the tunneling spectra of semiconductor band onsets is pictured in Fig. 3(c), in which tailing of the wave functions occurs through a barrier region of the semiconductor. This phenomenon has been shown previously to have a large impact on the form of the tunnel current near the onset of a bulk band.[1] We evaluate this effect here by explicit computations of the voltage dependence of the tunnel current. Our starting point for this computation is the WKB solution for the tunnel current of a planar barrier, as given by[1,24]

$$J = \frac{2e}{h}\int_{-\infty}^{\infty} dE[f(E) - f(E - eV)] \int \frac{d^2k_{\|}}{(2\pi)^2} D(E,k_{\|}), \quad (2)$$

where $f(E)$ and $f(E-eV)$ are Fermi-Dirac occupation factors for the sample and tip, respectively, $k_{\|}$ is the parallel wave vector, and $D(E,k_{\|})$ is the tunneling transmission term through the barrier. We assume that this formula can be applied to our case of a probe-tip in proximity to a flat surface, for which we take the barrier to be described by the potential along the central axis of our problem (any errors due to this assumption are expected to be quite small since the potential contours in the semiconductor have relatively large radius of curvature for all cases of interest).[2,3] The integral over parallel wave vector in this equation is in general restricted by the band structures of both the sample and the probe-tip. However, for a usual metallic probe-tip with its band minimum about 8 eV below the Fermi level, the restriction will be determined by the band structure of the semiconducting sample itself. For effective mass bands, the values of parallel wave vector then extend from 0 to a maximum value of $[2m^*(E-E_C)/\hbar^2]^{1/2}$ for the conduction band ($E>E_C$) or $[2m^*(E_V-E)/\hbar^2]^{1/2}$ for the valence band ($E<E_V$).

The transmission term in Eq. (2) is taken to be a product of the transmission through the vacuum and that through any barrier occurring in the semiconductor, $D(E,k_{\|}) = D_V(E,k_{\|})D_S(E,k_{\|})$. Within the WKB approximation the transmission factor for a trapezoidal barrier in the vacuum is given by

$$D_V(E,k_{\|}) = \exp(-2\kappa s), \quad (3a)$$

where s is the sample-tip separation and with

$$\kappa = \left[\frac{2m}{\hbar^2}\left(\bar{\phi} + E - E_F - \frac{eV}{2}\right) + k_{\|}^2\right]^{1/2}, \quad (3b)$$

where $\bar{\phi}$ is the average work function of the sample and tip. The effect of wave function tailing through the potential barrier in the semiconductor can be described by a transmission term of the form[1]

$$D_S(E,k_{\|}) = \exp\left[-2\int_A^B \left(\frac{2m^*}{\hbar^2}|E_i + \phi(z) - E| + k_{\|}^2\right)^{1/2} dz\right], \quad (4)$$

where A and B are turning points for the integral, E_i is the energy of the relevant band edge, and $\phi(z)$ is the electrostatic potential energy in the semiconductor with $\phi(z)\to 0$ far inside the semiconductor.

In the formulation of Eqs. (2)–(4), matching of the wave functions at the interfaces has been neglected. For effective mass bands and a planar barrier, and ignoring band bending in the semiconductor for a moment, this matching yields an additional term in the integrand of Eq. (2) given by[25]

$$\frac{16\kappa^2 k_S k_M \alpha}{(\alpha^2\kappa^2 + k_S^2)(\kappa^2 + k_M^2)}, \quad (5)$$

where k_S and k_M are perpendicular components of the wave vectors of the semiconducting sample and metallic probe tip, respectively, and $\alpha = m^*/m_0$ is the ratio of effective mass to free-electron mass. Evaluation of k_M requires knowledge of the location of the bottom of the conduction band for the metal; we take this to be 8 eV below the Fermi level, a typical value for a simple metal [Eq. (5) depends only weakly on this value for the energies of interest].

Equation (5) is inapplicable when a barrier in the semiconductor is present, and within the WKB approximation it would be necessary to derive more complicated expressions including matching across both the semiconductor propagating and barrier regions and the semiconductor and vacuum barrier regions. A more direct method however, and one that we utilize here, is to perform a numerical integration of the Schrödinger equation along the entire length of the potential variation,[13,14] i.e., from deep inside the semiconductor all the way to the probe tip, taking care to include the effective mass of the semiconductor in the matching conditions at the vacuum/semiconductor interface. We start with an outgoing wave on one far side (denoted by subscript 2) of the tunnel junction, and then integrate back through the junction to determine the amplitude of the incoming wave on the other far side (subscript 1). Denoting the wave vectors, effective masses, and amplitudes on either side as k_1, m_1, A_1, and k_2, m_2, A_2, respectively, the transmission term appearing in Eq. (2) is then given by $(k_2/k_1)(m_1/m_2)|A_2/A_1|^2$.

We make an explicit computation of the tunneling current, for a potential profile $\phi(z)$ obtained from a finite-element computation of band bending. For illustrative purposes we compare this result with that obtained by *neglecting* the wave function tails, i.e., by taking the transmission to be zero whenever a state encounters a nonzero barrier in the semiconductor. An example of such results are shown in Fig. 6,

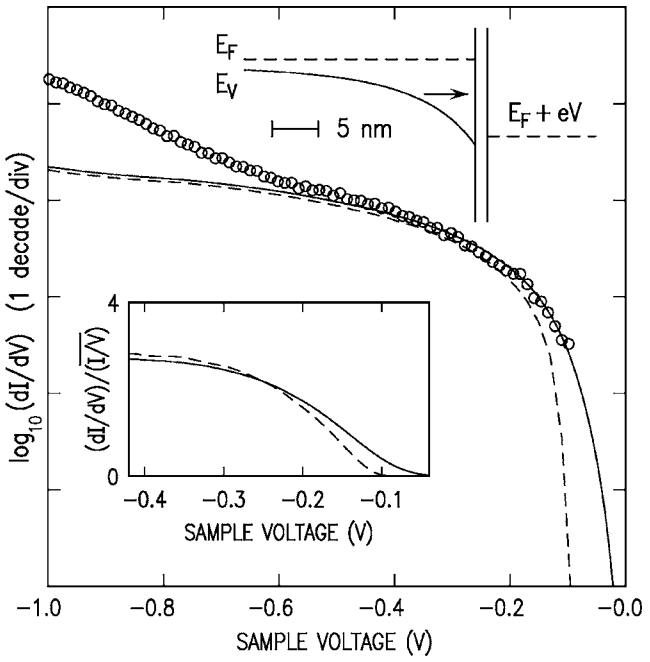

FIG. 6. Conductance at constant sample-tip separation for the spectral region near the VBM, comparing simulated results with (solid line) and without (dashed line) quantum effects, along with experimental data (open circles). The lower inset shows computed $(dI/dV)/\overline{(I/V)}$ curve for the simulated results. The upper inset shows the potential profile from the simulations at a sample-tip voltage of −0.111 V, with the arrow indicating the transmission through the semiconductor depletion region that is included in the quantum simulations.

where we consider tunneling into the valence band of Ge using heavy- and light-hole bands with effective masses of $0.34m_0$ and $0.043m_0$, respectively, and with our best-fit parameters as listed in the top row of Table I (with the E_N value being the semiclassical one).

We see from Fig. 6 that the effect of the wave function tails is to produce some additional tunnel current; in particular, for small voltages near the onset we find additional current extending into the gap region. If we view the results in terms of normalized conductance[26] as shown in the lower inset of Fig. 6, we find from fits to the band edges [using Eq. (A6b) of the Appendix] onset voltages of −0.065V or −0.106V for the cases when the transmission through the semiconductor barrier is included or neglected, respectively. The latter value is quite close to the predicted onset according to Eq. (1) of −0.111V for these parameters, but the former values differ from that by 0.046V. Such quantum effects become even larger for contact potentials that are more negative, since more downwards band bending occurs in that case at the voltage corresponding to the VB onset.

Also shown in Fig. 6 is a comparison of the computed conductance-voltage curve for the quantum computation (solid line) with experimental data (open circles), using the same data as in Fig. 1 but in this case normalized to constant sample-tip separation. It should be noted that the onset values obtained for these theoretical and experimental curves agree to within 2 mV [that is, obtained by fitting $(dI/dV)/\overline{(I/V)}$ for both theory and experiment but using the *same* $\overline{(I/V)}$, obtained from the experiment, in both cases as described in the following paragraph],[27] so that this comparison is a meaningful one. The overall shape of the theory curve agrees well with the experiment data for voltages as low as about −0.4V, below which the contribution of the rest-atom states to the conductance become important.

One technical issue arises in our use of the normalized conductance for the present situation of the Ge(111)$c(2\times 8)$ surface. The spectrum for this surface contains a very large adatom band with onset at about +0.5V, as seen in Fig. 1. When computing $\overline{(I/V)}$, using a broadening of 1V, it turns out that this adatom band makes a non-negligible contribution to the resulting $\overline{(I/V)}$ even at voltages as low as −0.1V. This effect shifts the apparent onset in $(dI/dV)/\overline{(I/V)}$ of the VB by about 10 mV compared to that obtained if the adatom band is absent (i.e., if we only use a bulk Ge CB, as done above). To obtain the best comparison of the experimental and simulated VB onset voltages it is thus desirable to use an $\overline{(I/V)}$ in the simulations that matches the experimental quantity. For this purpose we could attempt a detailed simulation of the adatom band itself, but an easier approach is simply to use the experimental $\overline{(I/V)}$ (i.e., from the data of Fig. 1) for normalizing the computed dI/dV values. We follow this approach in all the results described in the following section.

The behavior of the potential profile shown in Fig. 6 is relatively simple, decreasing monotonically as a function of distance from far inside the semiconductor towards the surface. More complicated behavior can occur for positive contact potentials, in which $\phi(z)$ initially decreases as one approaches the surface from far inside the semiconductor but than increases near the surface. For contact potentials greater than about 0.4 eV this behavior leads to localized states, i.e., accumulation states associated with the heavy hole band, forming near the surface. Such states are *not* observed in our experiments [even though the dynamic range of the measurement is large and such localized states *have* been observed in other situations such as for GaAs (Ref. 28)], and hence these situations can be excluded from consideration. But, even for smaller positive contact potentials that do not lead to localized states but still have nonmonotonic behavior of the potential, the predicted band onsets according to Eq. (1) will still be in error, with the error having an opposite sign than for the situation of Fig. 6. The full theory described above utilizing numerical integration of the Schrödinger equation is applicable for all such situations, and computations based on that theory are made for each of the parameter sets considered below.

D. Determination of band gap

We now return to the analysis of Sec. IV B, but using for the case of bulk bands the full current-voltage analysis of the preceding section. Hence we match the observed onset of the VB with that obtained from the current-voltage computation [rather than matching the band bending values derived on the basis of Eq. (1)]. The next-to-last column of Table I lists the resulting values of E_N that yield a VB onset of −0.111 V. We then evaluate the band bending $\phi_{0,A}$ at the voltage of +0.495 V corresponding to the onset of the adatom band,

with the resulting values listed in the final column of Table I.

The quantum effect of wave function tailing through the semiconductor barrier region affects the analysis in two ways. First, in plots such as Fig. 4, the computed band bending for the VBM is shifted slightly below the data point due to the difference between the semiclassical and quantum onset voltages. (A similar type of full current-voltage analysis is in principle also necessary for the high lying CB onset at 1.01 V, but the uncertainty of this band bending value of this feature is sufficiently large so as to render this analysis unnecessary.) However these shifts amount to only about 20–30 meV, so that the ranges of tip radii and extrinsic state density determined from the semiclassical analysis of Fig. 4 can still be used. But the second effect of the quantum analysis is in the $\phi_{0,A}$ values themselves, in which case the quantum results *are* noticeably shifted from the semiclassical ones, as can be seen from Table I.

To restrict the contact potential values we return to the separation-dependence of Fig. 5. The predicted VB onset voltages are modified due to the quantum effects, with the resulting dashed curves in Fig. 5(b) showing a significantly reduced separation dependence compared to the semiclassical results. From Fig. 5(a) a best-fit value of contact potential was found in Sec. IV B to be about -0.4 ± 0.2 eV. This range also appears to be consistent with the quantum results of Fig. 5(b), although the scatter in that data prevents any further discrimination of the value. We therefore use this range of -0.4 ± 0.2 eV for the contact potential, and the resulting parameter sets and $\phi_{0,A}$ values are listed in the final two rows of Table I. We note that the values of charge neutrality level for the semiclassical results in Table I fall substantially below the VBM, a situation that we cannot exclude but seems slightly unphysical, but in any case for the quantum analysis the situation changes and these values are quite close to the VBM.

Examining the entries in the final column of Table I, we find a range of $\phi_{0,A}$ extending from 4 to 35 meV. We have also considered variations in the values of more than one parameter, but still maintaining an overall band bending curve that falls within the range of curves *b* and *c* in Fig. 4. In this way we find a slightly larger range of $\phi_{0,A}$ values that are consistent with experiment, namely, −4 to 40 meV. Finally, we also consider the errors of ±0.010 V on the VBM onset value and ±0.003 V on the 0.495 V adatom-band onset that were used for matching; recomputing our results using the extremal values of these quantities leads to a range of $\phi_{0,A}$ value of −11 to 42 meV. Thus we arrive at a final value for the surface gap of 0.490 ± 0.027 eV, or in round figures, 0.49 ± 0.03 eV.

V. CONCLUSIONS

In summary, we have used STS to determine the surface band gap of the Ge(111)$c(2\times8)$ surface, i.e., the energy difference between the bulk VBM and the minimum of the adatom-induced surface band. Measurements were performed over a temperature range of 7–61 K, although the data are averaged together (and no systematic variation with temperature is observed) so that our result represents the gap at ≈30 K. The surface gap is found to have a width of 0.49 ± 0.03 eV.

In prior work, Büchel and Lüth used surface photovoltage measurements to determine onsets at 0.4 and 0.45 eV with the band associated with the first onset being apparently much smaller than that for the second.[6] More recently, Popik *et al.* observed numerous features within the bulk gap using low-energy electron backscattering, and one feature at 0.48 above the VBM was argued to correspond to a *maximum* in the empty state density.[7] Their discussion relied on comparisons with earlier works, although most of these (except for the work of Büchel and Lüth just mentioned) actually involved measurement on the Ge(111)2×1 surface rather than the $c(2\times8)$ surface. We therefore consider the surface photovoltage onsets at 0.4 and 0.45 eV to be the most reliable prior measurement of the surface gap.

The difference between the two previously observed onsets is somewhat smaller than the energy difference associated with the states of the two inequivalent Ge adatoms [about 0.15 eV in STS (Ref. 3) or 0.2 eV from theory[17]], and additionally the band associated with the first onset appears to be very much smaller than that associated with the second. For that type of optical experiment it must also be kept in mind that excitonic effects can produce a gap lowering; for the surface gap of Ge(111)2×1 surface this exciton binding amounts to about 0.2 eV, although it should be realized that the exciton in that case forms between bonding and antibonding state of similar nature (i.e., associated with π-bonded chains[11]) as opposed to the present case of a transition from a bulklike VB state to an adatom-derived surface state. In any case, we tentatively associate the lower onset at 0.4 eV with defect-induced states on the surface, i.e., the same as the extrinsic states seen in our STS and STM work, the presence of which is inherent to the formation of the $c(2\times8)$ reconstruction from the cleaved 2×1 surface.[15] We further associate the 0.45 eV value with the surface gap, with the small difference between that result and our value of 0.49 ± 0.03 eV possibly involving an excitonic effect.

We close with several comments on the methodology of this work. We have pursued here an analysis based in large part on the semiclassical notion of band bending, i.e., using Eq. (1). This type of analysis could be called an *energy alignment* method, and its utilization is quite simple since only values of the potential (not the tunneling current) are required. On the other hand, quantum effects are certainly present in the real physical situation; in the present case these are found to be quite small, but in other situations they may be larger. For example, in a recent reanalysis of STS data from InGaP/GaAs heterojunctions[29] it has been found that due to the large values of contact potential and the relatively restricted voltage-range of the spectra that the quantum effects dominate the band onsets, and consequently an energy alignment type of analysis fails. In that case one must compute tunneling current-voltage characteristics over the entire spectrum and match those to the observed spectra, in a type of *line shape analysis*. The theory presented in this work enables that type of analysis.

Our theory for computation of tunnel currents has focused on *bulk* bands, but it can also be extended in a straightforward way to the case of *surface* bands using some model for

the surface state dispersion (e.g., as in Ref. 30, but with the energies of the surface states shifted by ϕ_0). Of course, in reality, resonant bands have mixed surface and bulk character, but in the absence of a detailed local-state-density computation one would not know the precise nature of each given state. Hence, in a typical simulation of the type described here one must assume that a given band has either surface or bulk character. For our present computations we have assumed the states associated with the VB feature in the spectra to have bulk character, although some prior experiments have shown it to have partial surface character (i.e., as expected through mixing with rest-atom derived states).[5] This assumption does however *not* lead to any additional uncertainty in our derived surface gap, since even for the extreme opposite assumption of full surface character for the VB feature the resulting analysis would just proceed utilizing Eq. (1), with the results being the semiclassical ones listed in Table I. Those results do not differ significantly from the quantum ones within the error range of our final result, although the former do tend to favor gap values in the lower part of that range.

Finally, we note that the analysis of this work has proceeded with the assumption that the extrinsic states on the surface can be treated as spatially uniform, whereas we know that they primarily originate from $c(2\times8)$ domain boundaries that are located 10–20 nm from the point at which spectra are acquired. To evaluate the consequence of this assumption we have redone our analysis using a model in which there are no extrinsic states for a radius of 10 nm from the central axis of the problem, and for larger radii we assume a density that is an order-of-magnitude larger than 4×10^{12} cm^{-2} eV^{-1} such that the computed band bending curves are very similar to those of Fig. 4. The charge neutrality levels needed to match the VB onset then shift slightly compared to those of Table I, and the resulting $\phi_{0,A}$ values are about 9 meV less than those listed in the table. This effect is thus small, and does not significantly impact our final result for the surface gap. The same conclusion also applies to the assumed energy uniformity of the spectrum of extrinsic states: We know experimentally that these states are reasonably well distributed over the gap;[3] this observation, coupled with the fact that the tip-induced band bending varies with distance from the tip (so that at any particular voltage the surface Fermi-level intersects the spectrum of extrinsic states at a different energy for each distance), again leads to a negligible sensitivity of our final result on the energy nonuniformity of the extrinsic states.

APPENDIX: BAND EDGE DETERMINATION USING NORMALIZED SPECTRA

In the past, our spectroscopic normalization was used primarily as a qualitative means of analysis, enabling the spectra to be viewed on a linear (rather than logarithmic) scale. In the present work, however, we have used the normalized conductance in a more quantitative way in order to determine band edge energies. For this purpose, a careful reexamination of the analysis procedure is needed. We accomplish that here by using *simulated* current and conductance characteristics,

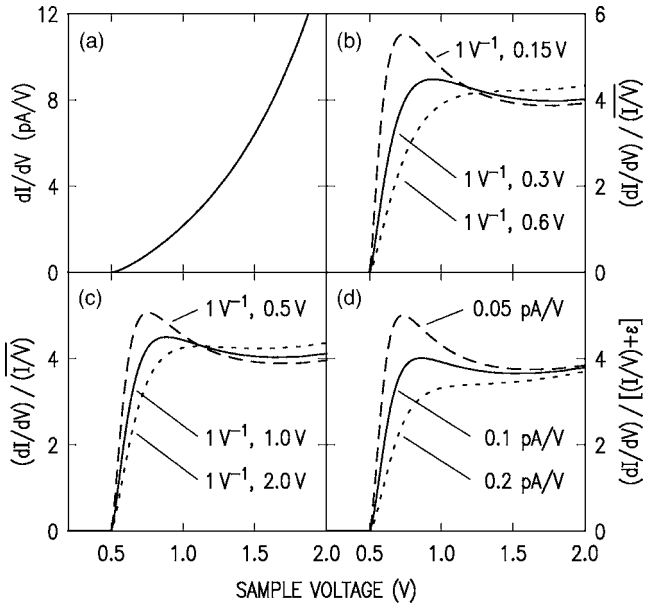

FIG. 7. Comparison of various methods for spectroscopic normalization: (a) Simulated curve of dI/dV based on tunneling at a temperature of 10 K into an effective-mass band with onset at +0.5 V. (b) Normalization performed by convolution of I/V with exponential function, for the values of a' and $\Delta V'$ indicated. (c) Normalization performed by convolution of I/V with function composed of sine and cosine integrals, for the values of a' and ΔV indicated. (d) Normalization performed by addition of a constant to I/V, for the values of ε indicated.

using the formulas described in Sec. IV C for tunneling from a metal probe-tip into a semiconductor effective-mass band, and neglecting tip-induced band bending [Eq. (4)]. Near a band edge, the vacuum transmission term of Eq. (3) can be approximated as being independent of energy. Neglecting the boundary matching term of Eq. (5), the integral of Eq. (2) is then easily evaluated to yield a quadratic voltage dependence of the current and hence a linear voltage dependence for the conductance. Including Eq. (5) however yields a voltage onset of the conductance varying with a 3/2 power;[31] this behavior persists to higher voltages, and comparing with experimental data[1,33] we find better agreement with the theory when this term is included. In Fig. 7(a) we plot such an onset, computed using a temperature of 10 K, sample-tip separation of 0.9 nm, effective mass of $0.1m_0$, conduction band onset of +0.5 V, and assuming a tunnel junction area of 1 nm^2. The rather nonlinear behavior of the onset is clearly seen in the figure.

Let us now consider use of the normalized conductance $(dI/dV)/(\overline{I/V})$ rather than simply dI/dV. Phenomenologically, this normalized conductance has been found to produce what appear to be well-defined band edges with linear onset behavior.[32,33] In this normalization, $(\overline{I/V})$ is formed by broadening of (I/V) through convolution with some suitable function [this broadening is necessary since, near a band edge, the current approaches zero faster than the conductance and in the absence of any broadening the ratio $(dI/dV)/(I/V)$ diverges at a band edge]. We examine the normalization procedure in detail here, using various methods to accomplish it.

We first consider broadening using an exponential convolution function, $\exp(-|V|/\Delta V')/(2\Delta V')$, where $\Delta V'$ is the broadening parameter. As described in Ref. 33 we include a scaling function $\exp(-a'|V|)$ multiplying (I/V) such that the convolution, at some voltage V, weights voltages above and below V approximately equally. An appropriate value of a' is given by the voltage dependence of the tunnel barrier transmission term,[14] $\exp\{-2s[2m(\bar{\phi}-e|V|/2)]^{1/2}/\hbar\}$. Equating this form to $\exp\{-2s[2m\bar{\phi}]^{1/2}/\hbar\}\exp\{a'|V|\}$ yields, to lowest order in V, $a' \approx es[m/(2\bar{\phi})]^{1/2}/\hbar \approx 1\ \mathrm{V}^{-1}$. The complete formula for $\overline{(I/V)}$ is then given by

$$\overline{(I/V)} = \exp(a'|V|)\frac{1}{2\Delta V'}\int_{-\infty}^{\infty}[I(V')/V'] \times \exp\left(\frac{|V-V'|}{\Delta V'}\right)\exp(-a'|V'|)dV'. \quad \text{(A1)}$$

Normalized spectra computed using this method are shown in Fig. 7(b), with various values of $\Delta V'$ and using the simulated conductance vs voltage curve of Fig. 7(a). For the purpose of the normalization it is necessary to assume a valence band (at negative voltages), which we take to have an effective mass of $0.1m_0$ and onset of -0.5 V.

We take this opportunity to point out a significant difference between the convolution method *discussed* in Ref. 33 and the analysis method that was actually *used* in that work. The difference between the methods is most easily described in terms of Fourier analysis, which in practice is how we compute the convolutions.[32] The Fourier transform of the scaled (I/V) is multiplied by the Fourier transform of the convolution function, and an inverse transform is then made of this product, which after inverse scaling yields $\overline{(I/V)}$. Let us denote by f the frequency variable conjugate to voltage. The Fourier transform of the exponential convolution function is given by

$$\frac{1}{1+f^2/f_0^2} \quad \text{(A2a)}$$

with

$$f_0 = \frac{1}{2\pi\Delta V'}. \quad \text{(A2b)}$$

Although this exponential broadening method was explicitly discussed in Ref. 33 we have recently realized that the method actually implemented in the computer program used there is *not* given by Eq. (A2). Rather we have used (in Ref. 33 and in all subsequent works) the following form:

$$\frac{1}{1+|f|/f_0} \quad \text{(A3a)}$$

with

$$f_0 = \frac{1}{\Delta V}. \quad \text{(A3b)}$$

There are two discrepancies in this form compared to Eq. (A2)—the power of 2 on the frequency in Eq. (A2a) is only a linear power in Eq. (A3a), and the factor of 2π in the denominator of Eq. (A2b) is absent in Eq. (A3b). This second discrepancy can be easily accommodated simply by taking ΔV to be $2\pi\Delta V'$. The first discrepancy is potentially more significant, but we find from a comparison of normalized spectra computed using Eqs. (A2) and (A3) that the methods produce very similar results so long as the f_0 parameter in the latter case is about 2 times greater then that of the former. Combined with the previous factor of 2π, we find that the normalization methods expressed by Eqs. (A2) or (A3) are nearly equivalent so long as $\Delta V \approx 3\Delta V'$.

For completeness, we derive the convolution-function corresponding to Eq. (A3). This is given by its inverse Fourier transform, which we evaluate to be $2g(2\pi|V|/\Delta V)/\Delta V$ where $g(x)$ is an auxiliary function to the sine and cosine integrals $\mathrm{Si}(x)$ and $\mathrm{Ci}(x)$, given by $g(x) = -[\sin(x)\mathrm{si}(x) + \cos(x)\mathrm{Ci}(x)]$ with $\mathrm{si}(x) = \mathrm{Si}(x) - (\pi/2)$.[34] Efficient algorithms for evaluating $g(x)$ are known.[34] The function $g(x)$ for $x>0$ decreases monotonically with x. It diverges logarithmically as $x\to0$, and it decreases relatively rapidly with x up until $x\approx1.2$ where it is comparable in magnitude to $\exp(-x)$. For larger values of x it decreases relatively slowly, varying asymptotically as $1/x^2$. The median values for $g(x)$ and $\exp(-x)$ for $x>0$ are comparable, being $x\approx0.62$ for the former and $x=0.693$ for the latter. With this form for the convolution function, the formula for $\overline{(I/V)}$ computed according to this second normalization method is given by

$$\overline{(I/V)} = \exp(a'|V|)\frac{2}{\Delta V}\int_{-\infty}^{\infty}[I(V')/V']g\left(\frac{2\pi|V-V'|}{\Delta V}\right) \times \exp(-a'|V'|)dV'. \quad \text{(A4)}$$

Normalized spectra obtained using this method are shown in Fig. 7(c). We see that the results of Figs. 7(b) and 7(c) are nearly identical, so long as one includes the factor of 3 between their respective broadening parameters.

We also show in Fig. 7(d) the results for a third type of normalization, in which we compute simply $(dI/dV)/[(I/V)+\varepsilon]$ where ε is a parameter. Again, very similar results are obtained as with the other normalization methods, for appropriate values of the parameters. The methods of Figs. 7(b) and 7(c) each have two parameters as compared with a single parameter for the method of Fig. 7(d), which is an apparent advantage of the latter. However, as discussed in Ref. 33, the former two methods can be applied in combination with the acquisition method of variable sample-tip separation such that the analysis involves only a single parameter. Also, these two methods can be applied to any data set using nearly invariant parameter values, whereas the method of adding ε to the denominator requires a different parameter value for different ranges of the conductance. In any case there is no large difference between the results of the various methods; for consistency with our past results we continue our use of Eq. (A3) for normalization of our spectra.

Referring again to Fig. 7, it is apparent that a good choice of parameter values in the normalization is that which produces the solid lines in each of Figs. 7(b)–7(d), i.e., in which

the edge of the band is quite sharp and linear but for which no significant overshoot occurs at the edge. It is thus seen how the normalization produces some *linearization* of the band edge. Having found this behavior, we seek a simple functional form, which includes temperature dependence, to describe such an onset. To derive this we first write the tunnel current in a very approximate manner as

$$I \propto \int_{-\infty}^{\infty} [f(E) - f(E - eV)]\rho_S(E)dE, \tag{A5}$$

where $\rho_S(E)$ is an *effective* state density for the sample which includes the effect of the vacuum transmission factor in selecting states over a certain range of $k_\parallel$ values (we are assuming a constant tip state density here). To obtain a linear dependence of conductance on voltage we then use a linearly increasing sample state density, $\rho_S(E) \propto (E - E_F - eV_0)\theta(E - E_F - eV_0)$ where eV_0 is the onset energy of the band relative to the sample Fermi level, and $\theta(E)$ is a step function. Assuming that the band onset is well separated from the sample Fermi level, the resulting form for the conductance is found to be

$$G(V) = C\int_{eV_0}^{\infty} \frac{dE}{1 + e^{(E-eV)/kT}} \tag{A6a}$$

$$= C[(V - V_0) + \beta \ln(1 + e^{-(V-V_0)/\beta})], \tag{A6b}$$

where $\beta \equiv kT/e$ and with C being a parameter. These equations are suitable for a conduction band extending over $E - E_F > eV_0$; the appropriate form for a valence band extending over $E - E_F < eV_0$ can be obtained by replacing both occurrences of $(V - V_0)$ in Eq. (A6b) by $(V_0 - V)$. As discussed above, we perform fits to the normalized conductance rather than to dI/dV itself, since it is the former that has the most linear behavior near a band edge.

We show in Fig. 8 results of fitting this functional form to the simulated curves of the normalized conductance [the normalization being performed using Eqs. (A3), with $a' = 1\ \mathrm{V}^{-1}$ and $\Delta V = 1$ V]. We perform the fits over values of normalized conductance values over the range 0 to 2.0. For the simulated spectra at temperatures of 10, 100, 200, and 300 K, respectively, the results for the V_0 parameter of the fits are 0.508, 0.506, 0.502, and 0.493 V for the +0.5 eV onset and −0.509, −0.508, −0.507, and −0.505 V for the −0.5 eV onset. The discrepancy between the fit results and the actual onsets are thus less than 10 mV in all cases. In contrast, if we simply fit the $T=0$ form to the 300 K results we obtain for the +0.5 eV onset an error of 38 mV. These results are fairly independent of the parameters a' and ΔV used for the normalization; varying either of these values by a factor of two produces only small changes (5 mV at 10 K, and 15 mV at 300 K) to the fit results.

To fully describe the observed band onsets we also consider the additional broadening effect of the modulation voltage used for the data acquisition. The measured conductance

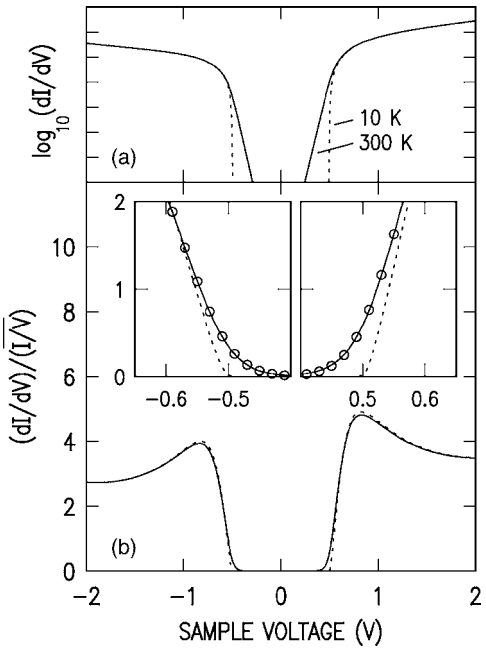

FIG. 8. Simulation of tunneling spectra for tunneling into effective mass bands, with onsets at ±0.5 V. The computed spectra are displayed as (a) conductance at constant sample-tip separation (one decade per division) and (b) normalized conductance on a linear scale, and results are shown for temperatures of 10 K (dotted lines) and 300 K (solid lines). The insets in (b) show an expanded view of the band onsets, with circles indicating a fit to the 300 K onset using a functional form that includes the temperature dependence of the normalized conductance.

is obtained from the input signal, $I(V)$, according to the actions of the demodulator and integrator in the lock-in amplifier as given by

$$\frac{dI}{dV} = \int_0^{2\pi} \frac{\sin\theta d\theta}{\sqrt{2}V_{\mathrm{rms}}\pi} I(V + \sqrt{2}V_{\mathrm{rms}}\sin\theta), \tag{A7}$$

where V_{rms} is the rms modulation voltage used in the measurement. We therefore perform simulations using this form for dI/dV rather than the numerical derivative of $I(V)$ as done for the simulations in Fig. 8. The results (not shown) do indeed display additional broadening at the onset. We fit the simulated results using the form given by Eq. (A6b), but with a modified value for β which we take to be

$$\beta = [(kT/e)^2 + (cV_{\mathrm{rms}})^2]^{1/2}, \tag{A8}$$

where c is a parameter. We choose a value for c such that the fits based on Eq. (A6b) accurately reproduce the simulated normalized conductance. Considering temperatures in the range 10–300 K and for V_{rms} values as large as 50 mV, we find an optimal value for c of about 0.4. The errors in the onset voltages V_0 thus obtained have magnitude of about $0.15V_{\mathrm{rms}}$ over and above that from the temperature dependence alone. In contrast, if no accommodation is made for the modulation voltage then this additional error is about $0.5V_{\mathrm{rms}}$.

*Electronic address: feenstra@cmu.edu
†Present address: IBM Research Division, Zurich Research Laboratory, 8803 Rüschlikon, Switzerland.

[1] R. M. Feenstra and J. A. Stroscio, J. Vac. Sci. Technol. B **5**, 923 (1987).
[2] R. M. Feenstra, J. Vac. Sci. Technol. B **21**, 2080 (2003).
[3] R. M. Feenstra, G. Meyer, and K.-H. Rieder, Phys. Rev. B **69**, 081309(R) (2004); R. M. Feenstra, S. Gaan, G. Meyer, and K.-H. Rieder, *ibid.* **71**, 125316 (2005). There is a typographical error in the labeling of Fig. 10, the horizontal axis label should be the negative of that shown.
[4] R. S. Becker, B. S. Swartzentruber, J. S. Vickers, and T. Klitsner, Phys. Rev. B **39**, 1633 (1989).
[5] J. Aarts, A. J. Hoeven, and P. K. Larsen, Phys. Rev. B **37**, 8190 (1988), and references therein.
[6] M. Büchel and H. Lüth, Surf. Sci. **50**, 451 (1975).
[7] T. Yu. Popik, V. M. Feyer, O. B. Shpenik, and Yu. V. Popik, Surf. Sci. **491**, 175 (2001).
[8] F. J. Himpsel, Surf. Sci. Rep. **12**, 1 (1990).
[9] P. Molinàs-Mata, A. J. Mayne, and G. Dujardin, Phys. Rev. Lett. **80**, 3101 (1998).
[10] G. Dujardin, A. J. Mayne, and F. Rose, Phys. Rev. Lett. **89**, 036802 (2002).
[11] M. Rohlfing, M. Palummo, G. Onida, and R. Del Sole, Phys. Rev. Lett. **85**, 5440 (2000).
[12] R. M. Feenstra, G. Meyer, F. Moresco, and K. H. Rieder, Phys. Rev. B **64**, 081306(R) (2001).
[13] R. S. Becker, J. A. Golovchenko, and B. S. Swartzentruber, Phys. Rev. Lett. **55**, 987 (1985).
[14] R. M. Feenstra, J. A. Stroscio, and A. P. Fein, Surf. Sci. **181**, 295 (1987).
[15] R. M. Feenstra and A. J. Slavin, Surf. Sci. **251/252**, 401 (1991).
[16] E. S. Hirschorn, D. S. Lin, F. M. Leibsle, A. Samsavar, and T.-C. Chiang, Phys. Rev. B **44**, R1403 (1991).
[17] N. Takeuchi, A. Selloni, and E. Tosatti, Phys. Rev. Lett. **69**, 648 (1992).
[18] J. P. Perdew, K. Burke, and M. Ernzerhof, Phys. Rev. Lett. **77**, 3865 (1996).
[19] N. Troullier and J. L. Martins, Phys. Rev. B **43**, 1993 (1991).
[20] J. Y. Lee and M. H. Kang, Phys. Rev. B **66**, 233301 (2002).
[21] *Semiconductors: Group IV Elements and III-V Compounds*, edited by O. Madelung (Springer-Verlag, Berlin, 1991).
[22] Our data was acquired over the temperature range of 7–61 K, with values of E_F-E_V for Ge with 2×10^{16} cm^{-3} p-type doping varying between 5 and 19 meV over this range, assuming a shallow acceptor level of 10 meV. We use a typical temperature of 30 K in our computations corresponding $E_F-E_V=10$ meV, with any systematic error due to the use of this fixed value being negligible compared to the other uncertainties in our results.
[23] R. D. Bringans, R. I. G. Uhrberg, and R. Z. Bachrach, Phys. Rev. B **34**, 2373 (1986).
[24] C. B. Duke, *Tunneling in Solids* (Academic, New York, 1969), Eq. (7.8).
[25] See Ref. 24, Eq. (18.31); W. A. Harrison, Phys. Rev. **123**, 85 (1961).
[26] The normalized conductance is computed here using bulk bands of Ge, i.e., with a CB located 0.74 eV above the VB and using the procedure of Eq. (A4) of the Appendix with parameters $a'=1$ V^{-1} and $\Delta V=1$ V.
[27] It is just a coincidence that the onset for this particular theory curve, whose parameters are chosen such that its semiclassical band onset is precisely −0.111 V, happens to closely agree with the onset of the particular experimental data set shown. Also, the purpose of the comparison between theory and experiment in Fig. 6 is *not* to illustrate that the full theory (solid line) is somehow better than the approximate theory (dashed line), but rather, only to show that the overall shape of the full theory curve agrees well with that of the experimental data.
[28] R. M. Feenstra, G. Meyer, F. Moresco, and K. H. Rieder, Phys. Rev. B **66**, 165204 (2002).
[29] Y. Dong, R. M. Feenstra, M. P. Semtsiv, and W. T. Masselink, Appl. Phys. Lett. **84**, 227 (2004).
[30] R. M. Feenstra, Phys. Rev. B **60**, 4478 (1999).
[31] C. B. Duke, *Tunneling in Solids* (Academic, New York, 1969), p. 55.
[32] P. Mårtensson and R. M. Feenstra, Phys. Rev. B **39**, 7744 (1989).
[33] R. M. Feenstra, Phys. Rev. B **50**, 4561 (1994).
[34] M. Abromovitz and I. A. Stegun, *Handbook of Mathematical Functions* (Dover, New York, 1965), p. 232.